ACS SyntheticBiology

pubs.acs.org/synthbio Research Article

Mutations in the Substrate-Binding Pocket of DiacylGlycerol Acyltransferase Alter the Fatty Acid Composition of Triacylglycerides in Yeast

Published as part of ACS Synthetic Biology special issue "Synthetic Biology in Food Production".

Nazreen V. M. Abdul Muthaliff,[†] Nur Eka Fitriani,[†] Derek Smith, Jing Sen Ong, Lay Kien Yang, Coleen Toledo Busran, Aaron Thong, Prakash Arumugam, and Naazneen Sofeo*

Cite This: https://doi.org/10.1021/acssynbio.5c00143 Read Online

ACCESS | Metrics & More | Article Recommendations | Supporting Information

ABSTRACT: Triacylglycerols (TAGs) are the main components of food oils and fats. The fatty acid composition of TAGs varies for different oils and fats. Specific enzymes sequentially add three fatty acids to the glycerol backbone of TAGs. Diacylglycerol acyltransferase or DGAT adds the third and ultimate fatty acid to the glycerol backbone at the *sn*-3 position. In this study, we characterized the substrate-binding pocket of enzyme DGAT1 from *Arabidopsis thaliana* through heterologous expression in the DGAT mutant of *Saccharomyces cerevisiae*. We performed site saturation mutagenesis on 10 amino acid residues in the catalytic site and examined their effects on the fatty acid profile of yeast cells. Our results indicate that mutations F373G, T240I, M289F, and V248I impact the yeast TAG profile either in terms of the total saturation level or the carbon chain length of the fatty acids, suggesting that they change the DGAT's substrate preference. This offers insights into crucial amino acid residues in the DGAT binding pocket which can be engineered for fine tuning the lipid profile. In summary, we have harnessed the power of enzyme engineering to modify the fatty acyl makeup of triglycerides and created a sustainable platform for the production of customized alternative lipids.

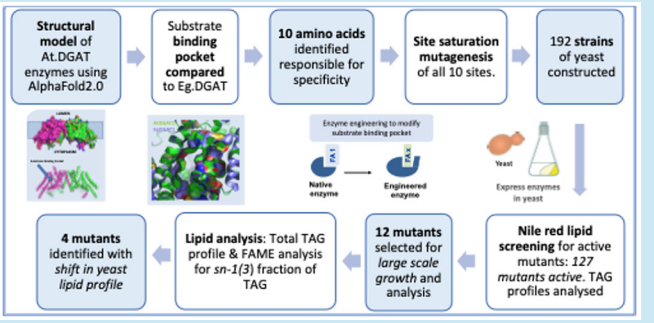

KEYWORDS: *lipids, triacylglycerol, DGAT enzyme, Arabidopsis thaliana, enzyme engineering, Saccharomyces cerevisiae*

INTRODUCTION

Lipids are crucial organic molecules that are essential for membrane integrity, cellular signaling, and energy storage.[1,2] Key lipid types, such as fatty acids, triglycerides, phospholipids, and sterols, play vital roles in maintaining cellular functions.[1,2] In food, lipids provide energy, aid in the absorption of fat-soluble vitamins, and enhance the flavor and texture while supporting immune function and vision.[1−3] Most food oils and fats are currently derived from animal and plant sources.[2,4] Traditional sources of fats and oils face challenges such as the rise in global population and looming climate crisis. This urgently calls for an alternative platform for production of different oils and fats to cater to the increasing demand.[5] Microbial lipids can serve as a sustainable source of oil since they are amenable to large-scale fermentation and can utilize various feedstocks.[6,7] Oleaginous yeasts like *Lipomyces starkeyi*, *Yarrowia lipolytica*, and *Rhodotorula toruloides* are excellent producers of lipids.[8]

Lipids, particularly dietary triacylglycerols (TAGs), are the primary form of fats consumed in the human diet, acting both as a key energy source and carriers of essential fatty acids.[9] TAGs are composed of three fatty acid chains esterified to a glycerol backbone.[9] The stereospecificity and composition of fatty acids in the TAG influence the functional, nutritional, and physical properties of fat in food.[10] Qualities like mouth-feel are dependent on properties such as the melting point. Lower melting point of chocolate is due to the presence of C18:1 at the *sn*-2 position and C16:0 and C18:0 at the *sn*-1/3 position.[10] In oils such as palm oil[10] and cocoa butter,[11] saturated fatty acids occur primarily at the *sn*-1 and *sn*-3 positions.

TAGs are synthesized from glycerol-3-phosphate (G3P) through a series of enzymatic steps. First, G3P is acylated by glycerol-3-phosphate acyltransferase using acyl-CoA to form

Received: February 26, 2025
Revised: August 21, 2025
Accepted: August 21, 2025

lysophosphatidic acid (LPA).[12,13] LPA is then further acylated by 1-acylglycerol-3-phosphate acyltransferase, resulting in the formation of phosphatidic acid. Phosphatidic acid is subsequently dephosphorylated by phosphatidate phosphatase to produce diacylglycerol (DG). Finally, DG undergoes acylation by diacylglycerol acyltransferase (DGAT), which adds a third fatty acyl group from acyl-CoA to form TAG.[12,13]

At least two classes of genes, *DGAT1* and *DGAT2,* encoding the key rate-limiting DGAT enzyme in TAG biosynthesis have been identified in plants.[13−16] DGATs have been shown to have impact on quality, composition, and yield of lipids[17−20] and hence is an interesting candidate for food and biotechnology applications.

The two plant DGATs exhibit distinct temporal and spatial expression patterns across plant organs and during different stages of development[21−23] DGAT1 and DGAT2 also display minor difference in substrate specificity.[21,23,24] For example, jatropha (*Jatropha curcas* L.) JcDGAT2 had a significant substrate preference to linoleic acid in both yeast and tobacco systems, as compared to JcDGAT1.[25] In tung tree (*Vernicia fordii*), DGAT2 displayed a modest preference for 18:3-CoA as the acyl donor.[21] DGAT1 from *Arabidopsis thaliana* has been shown to preferentially incorporate oleoyl-CoA (18:1)[17] and palmitic acid (16:0),[26] while DGAT2b from *Cyperus esculentus* prefers unsaturated fatty acids.[27] Interestingly, DGAT1 from *Elaeis guineensis* (oil palm) exhibits a marked preference for medium-chain fatty acids.[18] Advances in enzyme engineering have provided insights into the key sites responsible for TAG formation. Transgenic overexpression of S197A-mutated *Tropaeolum majus* DGAT1 (TmDGAT1) resulted in a 20−50% increase in the oil content.[28] Furthermore, the introduction of a phenylalanine insertion at position 469 (F469) in DGAT1-2 enhanced seed oil concentration and oleic acid levels in maize.[29] DGAT1 has been found to be the rate-limiting enzyme in TAG biosynthesis and has been the focus of various strategies to increase TAG production.[30−32]

Saccharomyces cerevisiae strain H1246 has been routinely used to study DGAT functionality and substrate preferences.[16,33,34] Heterologous overexpression of DGAT1 from different species in these yeasts has been used for improving TAG production and tuning the TAG fatty acid profile.[16] Engineering of enzymes involved in the fatty acid and TAG biosynthetic pathways has been used as a successful strategy to tune the carbon chain and saturation of lipid products.[18,35]

In this study, we report the heterologous expression of DGAT1 from *Arabidopsis thaliana* in the yeast *Saccharomyces cerevisiae* H1246 host. We examine the 3D structural model to identify the substrate-binding pocket for this plant protein and use automation to generate about 190 mutants. We perform total TAG analysis and *sn-1,3* FAME analysis to quantify the fatty acid profile changes caused by different DGAT mutations. Our data indicate that mutations in multiple amino acid residues of DGAT affect the TAG profile of yeast cells and provide insights into the crucial role of DGAT in determining the yeast TAG fatty acid composition. Changes to these amino acids altered the overall saturation level and carbon chain length of TAG produced by yeast cells.

MATERIALS AND METHODS

Strains, Materials, and Culture Media. The TAG-deficient *S. cerevisiae* strain H1246[36] (MATα are1-Δ::*HIS3* *are2*-Δ::*LEU2* *dga1*::*KanMX4* *lro1*-Δ::*TRP1* *ADE2* met ura3) was kindly provided by Prof. Sten Stymne (Scandinavian Biotechnology Research, Alnarp, Sweden). H1246 base strain was cultured in YPD medium (yeast extract 1%, peptone 2%, dextrose 2%) at 30 °C. Transformants were selected on synthetic defined drop-out media (ura$^-$) [6.7 g/L yeast nitrogen base without amino acids (Sigma Y0626), 1.92g/L yeast synthetic drop-out media supplements (Sigma Y1501), 2% (w/v) glucose]. For solid media, all components were the same except the addition of agar. Restriction enzymes, Gibson Assembly master mix (E2611), and Q5 hot start high-fidelity 2X master mix were purchased from New England Biolabs. PCR products were agarose gel purified using the E.Z.N.A Gel Extraction Kit (Omega Bio-Tek), and plasmids from *E. coli* were purified using E.Z.N.A Plasmid Mini Kit I (Omega Bio-Tek). Sequencing was performed by a vendor, 1st Base, Singapore.

Recombinant Plasmid Construction. The *A. thaliana* DGAT1 (At2g19450) cDNA sequence (AtDGAT) was codon-optimized with a C-terminal 6X-His tag and ordered from Integrated DNA Technologies (Supplemental Table S1). The uracil selection marker and the GAP promoter containing pESC vector were used (Supplemental Figure S1). Plasmid encoding AtDGAT cloned under the *GAP* promoter was transformed into Stellar Competent Cells (*Escherichia coli* HST08 strain) following manufacturer's protocol. Positive clones were confirmed through sequencing. Sequences of codon-optimized genes are listed in the supplemental data (Table S1). The codon-optimized sequences for CeDGAT2-2 (*Cyperus esculentus*),[37] TaDGAT2 (*Thraustochytrium aureum*),[38] OsDGAT1-1 (*Oryza sativa*),[39] and AtDGAT1 (*Arabidopsis thaliana*) were also cloned into the pYES2 vector under the inducible GAL1 promoter and transformed into *S. cerevisiae* H1246 cells.

Expression of DGAT in H1246 Yeast Strain. All yeast transformation into H1246 cells was performed using the standard lithium-acetate/PEG/single-strand DNA yeast transformation method.[40] For large-scale library transformations, the volume of reagents and the number of yeast cells were appropriately scaled up to accommodate the increased workload, ensuring optimal transformation efficiency and yield for the expanded scale of the experiment.

3D Structural Modeling and In Silico Analysis. Sequences for *Arabidopsis thaliana* DGAT1 (AtDGAT) and the medium-chain specific *Elais guineensis* DGAT1 (EgDGAT1-1) were obtained from the UniPROT database.[41] 3D dimeric models of the enzymes were generated using AlphaFold2-multimer[42,43] in ColabFold.[44] The models were viewed and manipulated using PyMOL.[45] Initial substrate/product docking was performed on AtDGAT using AUTODOCK Vina with oleoyl-CoA and 1-oleoyl-2-palmitoylglycerol as substrates and 1-oleoyl-2-palmitoyl-3-oleoylglycerol as the product. For the final choice of mutational positions, the two models were imported into PyMOL, and the publicly available script 'color_by_mutation.py' was used to identify all differing residue positions within the binding pocket. The 10 observed positions were chosen for site saturation mutagenesis.

Site Saturation Mutagenesis Library Creation using Automation. High-throughput restriction-free (RF) cloning for site-saturated mutagenesis was used to introduce precise changes to the wild type AtDGAT plasmid. Through a sequence-specific library of primers, mutations were performed. No restriction enzymes were used, and all liquid handling (except master mix preparations) and PCR cycling are performed on the SPARROW automation platform.

https://doi.org/10.1021/acssynbio.5c00143
ACS Synth. Biol. XXXX, XXX, XXX−XXX

Primers used for mutations are listed in supplemental data (Table S2). PCRs were carried out with iProof High-Fidelity DNA Polymerase (cat no. 1725301, Bio-Rad), miniaturized from manufacturer's protocols. A completely automated transformation protocol was also developed from a previously reported protocol and significantly miniaturized for use on the liquid handling platform.[40] A validation test was performed to confirm the transformation efficiency of known plasmids prior to full-scale testing. This validation aimed to confirm whether the miniaturized protocol could yield viable colonies while also quantifying the transformation efficiency and optimizing DNA input for full-scale transformation. Using 125 ng of plasmid DNA, over 200 colonies were obtained, suggesting that further miniaturization was possible by reducing the DNA input. In the final automated protocol, DNA input was adjusted to approximately 60 ng to maintain sufficient colony counts while preventing overcrowding in the smaller Omni-8 Agar Trays. All 192 mutant plasmids were successfully transformed into H1246 strains, and viable colonies were obtained. Three independent colonies were picked as biological replicates from each transformation except for M289Y which only gave two viable colonies upon transformation into H1246. Hence for obtaining the three replicates, one of the colonies for M289Y was grown twice.

Automated High-Throughput Nile Red Screening assay. Nile Red screening is a widely used fluorescence-based assay for detecting and quantifying neutral lipids and hydrophobic compounds in cells, tissues, and other biological systems. Nile Red screening was modified from an already reported protocol[46] and adapted to the SPARROW automation platform. The modified and adapted protocols are as follows. Preculture library (800 μL) was done in a 96-well deep well plate in SD-Ura media at 30 °C and 400 rpm for over 70 h until saturation. The cell density (OD_{595nm}) was measured in a 96-well F-bottom microplate (Greiner #655101), and a precalculated volume of preculture was taken to inoculate a culture library in 800 μL of SD-Ura media in technical duplicates along with six samples each of positive (wild type AtDGAT) and negative (Empty vector) controls, normalized to an OD_{595nm} = 0.1 in a 96-well deep well plate. This culture library was then cultured at 30 °C and 400 rpm over 48 h to accumulate lipids. All of the outer wells of plates were kept empty to reduce the effect of evaporation in samples. Before proceeding with the Nile Red assay, the cell density (OD_{595nm}) was measured again.

In the fully automated Nile Red screening assay, 150 μL of cell culture from each culture plate was taken to a new 96-well deep well plate, and the cells were collected by centrifugation at 500 × g for 2 min. The supernatant was discarded, and the cells were resuspended in 250 μL of 1× PBS wash. The wash step was repeated once more, with the addition of approximately 400 μL of 1× PBS wash to normalize the suspension OD_{595} = 1. 200 μL of the washed cells were taken for a final $OD_{595\ nm}$ measurement in a 96-well F-bottom black microplate (Greiner #655097), with blanks containing only 200 μL of 1× PBS.

For the measurement of the Nile Red fluorescence, 20 μL of 1:1 PBS:DMSO solution was first added to the washed cells in the same 96-well F-bottom black microplate. Subsequently, 20 μL of the Nile Red dye solution was added to the plate, with thorough pipet mixing. The plate was then immediately taken for a fluorescence read at 485/535 nm.

Lipid Analysis. All solvents used were analytical grade, unless stated otherwise. Chloroform, toluene solvent, boron trifluoride BF_3 in methanol solution, hydrochloric acid (HCl)) solution, TAG standard triundecanoyl glycerol, fatty acid methyl esters (FAME) standard solution, and Novozyme 435 lipase enzyme acrylic resin were purchased from Merck Co. (St. Louis, MO, USA). Diethyl ether, methanol, and ethanol solvents were acquired from Fisher Scientific (Seoul, Korea). HPLC grade n-hexane, sodium sulfate Na_2SO_4 anhydrous, and silica solid-phase extraction (SPE) cartridge Bond-Elut HF-SI were supplied by Honeywell, Goodrich Chemical Enterprise (GCE), and Agilent Technologies, respectively. For HPLC MS/MS mobile phase, organic solvents used were Optima LC/MS grade 2-propanol (isopropanol), HPLC grade methanol, and LC/MS grade formic acid from Fisher.

Extraction of TAG for HPLC MS/MS. To obtain the lipid extract, dried cultured biomass was extracted using methanol at 5 mg/mL. The mixture was shaken vigorously for 2 min followed by sonication for 45 min before centrifugation at 3000 rpm for 10 min. Subsequently, the supernatant was aliquoted and dried using a vacuum centrifuge and proceeded for HPLC MS/MS analysis.

Extraction of TAG sn-1,3 Fatty Acids. Fatty acids at positions 1 and 3 of TAG were hydrolyzed through enzymatic transesterification and subsequently isolated by fractionation using SPE cartridge according to Watanabe et al.,[47] with some modification. First, triundecanoyl glycerol C11:0 in TAG form was added into the sample as an internal standard (IS), and neutral lipid was extracted from the sample using the classical Folch method.[48] To approximately 200 mg of ground dried sample, 4 mL of chloroform/methanol (2:1, v/v) was added and vortex mixed, followed by sonication for 15 min. Subsequently, 0.8 mL of 0.05% NaCl solution was added to the mixture and centrifuged. The organic phase in the bottom layer was aliquoted, and another round of extraction was repeated on the remaining mixture. The combined extract was dried under a nitrogen stream. To the dried lipid, 100 uL of triundecanoyl glycerol (5 mg/mL) solution in chloroform was added as an IS. Next, 0.5 g of ethanol was added and mixed, followed by addition of 44 mg of Novozyme 435 lipase acrylic resin and vortex mixed. The mixture was subsequently placed in a shaking incubator at 250 rpm for 3 h for TAG transesterification, yielding 1,3 fatty acid ethyl esters (1,3 FAEE) and 2-monoacylglycerol. The sample was recovered by filtration using cotton and placed under a nitrogen stream for drying. To isolate 1,3 FAEE, the dried sample was reconstituted in 0.1 mL of hexane/diethyl ether (8:2, v/v) prior to loading a pre-equilibrated 50 mg silica cartridge. Next, the sample was eluted with 1 mL of hexane/diethyl ether (8:2, v/v), and the resulting fraction containing 1,3 FAEE was collected and dried using a nitrogen stream. Methylation of 1,3 FAEE was carried out by adding 200 μL of 14% w/v boron trifluoride in methanol and 100 μL of toluene following the AOAC 996.06 method. The final portion was recovered by adding 500 uL of water, 500 uL of hexane, and 0.1 g of sodium sulfate. The mixture was vortexed and allowed to settle. The hexane top layer was aliquoted into another vial containing 0.1 g of sodium sulfate for final water cleanup prior to injection.

Gas Chromatography Analysis. Methylated FAMEs were analyzed using capillary gas chromatography (GC) on an Agilent 7890 GC system (Agilent Technologies, Santa Clara, CA, USA) equipped with a hydrogen flame ionization detector according to AOAC 996.06 method[49] with slight modification.

https://doi.org/10.1021/acssynbio.5c00143
ACS Synth. Biol. XXXX, XXX, XXX−XXX

Into the capillary column SP2560 (100 m 0.25 mm 0.20 μm), 1 μL of sample test portion was injected at 25:1 split ratio with the following temperature program: injector, 225 °C; detector, 285 °C; initial oven, 100 °C, hold 4 min; ramp 3 °C/min; final oven, 240 °C, hold 17 min. The total FAME analysis for the lipids from the DGAT strains expressing various DGATs was performed based on AOAC 996.06 extraction method at 10 times smaller scale.[49]

GC Determination of TAG DGAT sn-1,3. Peak identification was carried out in reference to Supelco 37 Component FAME Mix standard solution (Merck Co. St Louis, MO, USA). Integration of the chromatogram peak was carried out using Agilent OpenLab CDS Chemstation Edition Rev. C.01.10[201]. Following the AOAC 996.06 method, each FAME was determined against IS.[50] Some modifications were applied to accounts for (1) the IS portion in the 1,3 FAEE fraction post enzymatic transformation (0.7182 × Wt_{istd}), and (2) the normalization against IS with conversion from FAEE to FAME (0.9346); thus, each FAME is determined as follows:

$$\mathrm{FAME}_i = \frac{\mathrm{Pt}_i \times 0.7182 \times \mathrm{Wt}_{\mathrm{istd}} \times 0.9346}{Pt_{\mathrm{istd}} \times R_i}$$

where FAME_i = fatty acid methyl ester *i* in the postfractionated portion of TAG DGAT; Pt_i = peak area of fatty acid of fatty acid *i* in the test portion; Wt_{istd} = weight of IS added in the test portion, g; Pt_{istd} = peak area of IS in the test portion; R_i = response factor for fatty acid *i*. Finally, FAME was converted to the fatty acid equivalent ($FA_{i,FAEE}$) using the corresponding conversion factor (f_{FAi}).

Liquid Chromatography-Mass Spectrometry. Dried lipid extracts were reconstituted in isopropanol/methanol (1:1, v/v) and shaken vigorously on a plate shaker for 20 min. The extracts were subsequently centrifuged at 3000 rpm for 10 min prior to analysis on an Agilent 1290 Infinity LC System coupled to an Agilent 6546 quadrupole time-of-flight (Q-TOF) mass spectrometer. 5 μL of extract was injected onto a Phenomenex Kitenex XB-C18 (2.6 μM, 150 × 2.1 mm). Mobile phases were methanol (A) and 2-propanol (B), both with 0.1% formic acid. The analysis was performed at a flow rate of 0.2 mL/min at 60 °C. The gradient was started at an initial composition of 8−20% B in 2 min, held for 1 min, followed by a linear increase to 25% B over 27 min, then to 80% B in 2 min, held for 3 min, and returned to the initial conditions. High-resolution mass spectrometry data were acquired in the positive electrospray ionization mode. Full MS1 scans were acquired between 225 and 1100 *m*/*z* at a scan rate of 2 spectra/s; while MS/MS spectra were acquired between 50 and 1500 *m*/*z* at a scan rate of 3 spectra/s, 8 precursors per cycle, and fixed collision energy of 45 eV. The typical Q-TOF operating parameters were as follows: sheath gas nitrogen, 12 L/min at 300 °C; drying gas nitrogen flow, 11 L/min at 300 °C; nebulizer pressure, 35 psig; nozzle voltage, 1.5 kV; capillary voltage, 3.5 kV. Lock masses in the positive ion mode: purine ion at *m*/*z* 121.0509 and HP-921 ion at *m*/*z* 922.0098. Software for data acquisition was Agilent Mass-Hunter Workstation LC/MS data acquisition, version 10.1 (Build 10.1.48). The percentages of different TAGs were calculated based on relative % of peak height for each strain.

LC-MS/MS Data Analysis. LC-MS/MS data analysis was performed using an in-house-developed Python script designed for the identification of TAG species. The script automates data processing, peak detection, and molecular annotation. The analysis pipeline integrates computational steps, including noise filtering at 100 count thresholds to eliminate artifact signal and isotope peak filtering at 5 ppm tolerance. Additionally, compound statements were employed for precursor and fragment ion searches with 10 ppm to enhance the confidence in TAG identification. The code was executed using Google Colab, leveraging Python libraries such as NumPy, Pandas, and Pyteomics for data handling and ProcessPoolExecutor to accelerate computation. Raw data were converted to mzML format using Proteowizard MSConvertGUI (64-bit) with applied filter of peak centroiding and subset MS level = 2. Each data point was searched against an in silico TAG library containing ion masses of diacyl glyceride (DAG) fragment(s) of a TAG constituent: DG [AA]+ for TAG AAA; DG [AA]+ and DG [AA]+ and [AB]+ for TAG AAB; and DG [AB]+, [BC]+ and [AC]+ for TAG ABC. Each match was registered as an identified TAG with precursor intensity and DAG fragment intensity recorded.

RESULTS AND DISCUSSION

Expression and Validation of Wild Type *Arabidopsis thaliana* DGAT1 Sequence (AtDGAT) in H1246 Strain. As *Arabidopsis thaliana* DGAT1 (AtDGAT) has been extensively studied to uncover its function and substrate specificity,[17,27,34,40] it was chosen for our study to characterize and engineer the DGAT's substrate-binding pocket. The full length sequence of *Arabidopsis thaliana* DGAT1 (At2g19450) was used. A codon-optimized sequence encoding the AtDGAT enzyme was successfully cloned into the pESC vector, which drives the expression of the transgene from the constitutive GAP (glyceraldehyde-3-phosphate dehydrogenase) promoter. The sequence-verified plasmid pESC-AtDGAT was transformed into *Saccharomyces cerevisiae* quadruple mutant H1246 strain (dga1Δlro1Δare1Δare2Δ). Functionality of the wild type AtDGAT enzyme was confirmed through Nile Red staining (Figure 1) and lipid analysis (Supplemental Figure S2). Untransformed H1246 cells and H1246 cells transformed with an empty pESC vector did not display any bright red fluorescent lipid droplets (Figure 1). In contrast, the H1246 cells transformed with pESC-AtDGAT exhibited bright red fluorescence spots, indicating neutral lipid production (Figure 1). This strongly suggested that AtDGAT is able to rescue the TAG biosynthesis deficiency of H1246 cells.

3D Structural Modeling and Identification of Sites for Mutagenesis. The three-dimensional structure of the AtDGAT dimer was modeled using AlphaFold. The structure is a member of the membrane-bound *O*-acyltransferase (MBOAT) family, similar to the published cryo-EM structure of human DGAT1 (PDB code 6VZ1).[51] The structure forms a homodimer through interactions involving part of the largely disordered N-terminus (residues 107−123) of the first monomer with the main domain of the second monomer as well as a hydrophobic interface between the monomers through dimerization across their respective first transmembrane helices (residues 133−158) (Figure 2A). Each monomer consists of nine transmembrane helices (TMs), with the N- and C-terminal regions located on the cytosolic and ER-luminal sides, respectively. The TMs form a large hydrophobic central cavity, which might act as the reaction center as established for the human DGAT1 (Figure 2B). This cavity has a lateral gate that opens to the membrane bilayer, facilitating the entry of lipid substrates directly from the membrane. A highly conserved histidine residue (H447)[52] is

https://doi.org/10.1021/acssynbio.5c00143
ACS Synth. Biol. XXXX, XXX, XXX−XXX

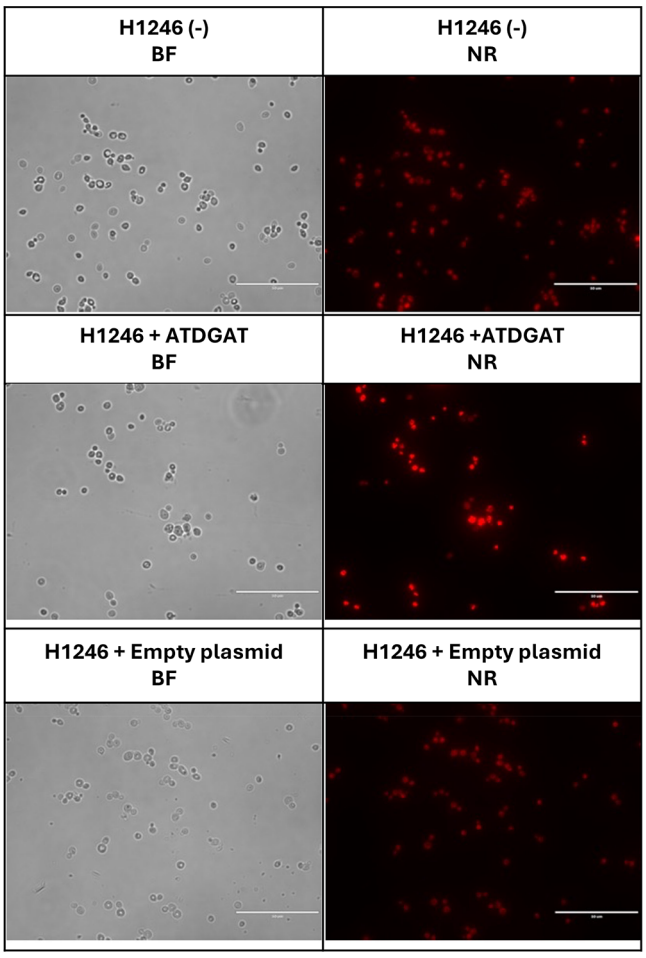

Figure 1. : Bright field (BF) and Nile Red stained fluorescence microscopy (NR) images of three strains. H1246 (−) indicates base *Saccharomyces cerevisiae* H1246 strain with no plasmid. H1246 + ATDGAT indicates H1246 strain with AtDGAT expressing pYES2 plasmid. H1246 + empty plasmid indicates H1246 strain with empty pYES2 plasmid.

buried inside the central cavity and plays a crucial role in the enzyme's catalytic mechanism by removing the proton from the diacylglycerol *sn*-3 hydroxyl, facilitating nucleophilic attack on the acyl-CoA carbonyl. The transition state is believed to be stabilized by hydrogen bonding with the side chain amide of an asparagine (N410) residue.[53,54]

To identify AtDGAT binding pocket positions for mutagenesis, initial molecular docking of oleoyl-CoA and 1-oleoyl-2-palmitoylglycerol as substrates and 1-oleoyl-2-palymitoyl-3-oleoylglycerol as a product was performed. However, the docking results were inconclusive, probably due to the extreme flexibility of the substrate and product, as well as the large cavity search space of the AtDGAT binding pocket. An alternative solution was chosen instead, where the AtDGAT would be directly compared with a homologous enzyme with a known differing substrate specificity. A structural model was generated of DGAT1 from *Elaeis guineensis* (EgDGAT1-1). This DGAT has a 60% amino acid sequence identity with AtDGAT and is known to prefer medium-chain fatty acid substrates (especially laurate).[18] The models were superposed and compared in PyMOL[45] to identify all positions that differ within the binding pocket (Figure 2B). A total of 10 positions near the substrate-binding pocket were identified through this method (F235, V239, T240, L244, I247, V248, M289, V290, M369, and F373 in the AtDGAT sequence) (Figure 2B).

Creation of Mutant Library. Ten amino acid residues identified were subjected to site saturation mutagenesis. Specific primers were designed to introduce targeted mutations into the AtDGAT coding sequence. A total of 192 sequence-verified plasmids were constructed that cover 19 mutations at each of the 10 sites (Supplemental Figure S3). Plasmids encoding the mutant AtDGATs were then introduced into *Saccharomyces cerevisiae* strain H1246. Three distinct *S. cerevisiae* transformants for each mutant were verified through colony PCR and stored as biological replicates.

Screening Mutant Library. Nile Red screening is a widely used fluorescence-based assay for detecting and quantifying neutral lipids and hydrophobic compounds in cells, tissues, or other biological systems.[46] Its ease of application and scaling also allow it to be used in microplate assays for screening large numbers of mutants. Hence, Nile Red staining was used to screen for DGAT mutants that are active. The background strain H1246 shows no-to-minimal fluorescence using Nile Red due to its inability to synthesize neutral lipids. If the mutant DGAT enzyme encoded by the transformed pESC plasmid is active, higher fluorescence is detected, whereas an inactive DGAT would result in no-to-minimal fluorescence like the base H1246 strain with an empty vector (Figure 1).

Of the 192 mutants created, Nile red staining and screening indicated that 65 mutants were inactive. 127 mutants showed fluorescence higher than the base strain H1246 (data not shown) and were chosen for further characterization. Most mutations to proline were inactive, except for V239 and L244. Top three amino acid residues with least number of active mutants (6−8) are M289, V248, and I247. This could be potentially be because these amino acid lines the edge of the lateral entry gate for the substrates (Figure 2B). Whereas, for amino acid residues F373 and T240, at least 16 out of 19 mutants were active. F373 and T240 lie at the lateral gate of the pocket; hence, its mutation potentially does not result in inactive mutants.

Lipid Profile Analysis of Mutants. All 127 mutants were subjected to LC-MS/MS analysis for deciphering the TAG composition. The high-throughput TAG composition analysis was initially done for a single replicate to prioritize the best candidates for a more detailed lipid analysis. The aim was to screen the best candidates for large-scale culture growth and lipid analysis. To identify the mutants with varied lipid profile, principal component analysis (PCA) was performed for the lipid profiles for these 127 mutants (Supplemental Figure S4). Twelve mutants that showed distinctive profiles were selected for the large-scale experiment. The selected mutants were F373G, F373M, F373W, F373N, V290F, V290I, M289Y, M289F, V248M, V248I, I247M, and T240I.

Large-scale cultures of the 12 selected mutants were grown and analyzed for total TAG profile and *sn-1(3)* FAME. 77 TAG molecular species were detected, all of them containing at least a single unsaturated site (no TAGs with saturated fatty acids at all three positions were detected). Figure 3 shows the PCA analysis performed based on the total TAG profile of these 12 mutants. From the PCA analysis, it is evident that most mutants show a clear shift in lipid profiles compared to the wild type. This shift could be in terms of the overall change of chain length, saturation levels, or total amount of TAGs produced. Since the growth rate and the resulting total lipid amounts varied for the mutants, the results for the lipid

https://doi.org/10.1021/acssynbio.5c00143
ACS Synth. Biol. XXXX, XXX, XXX−XXX

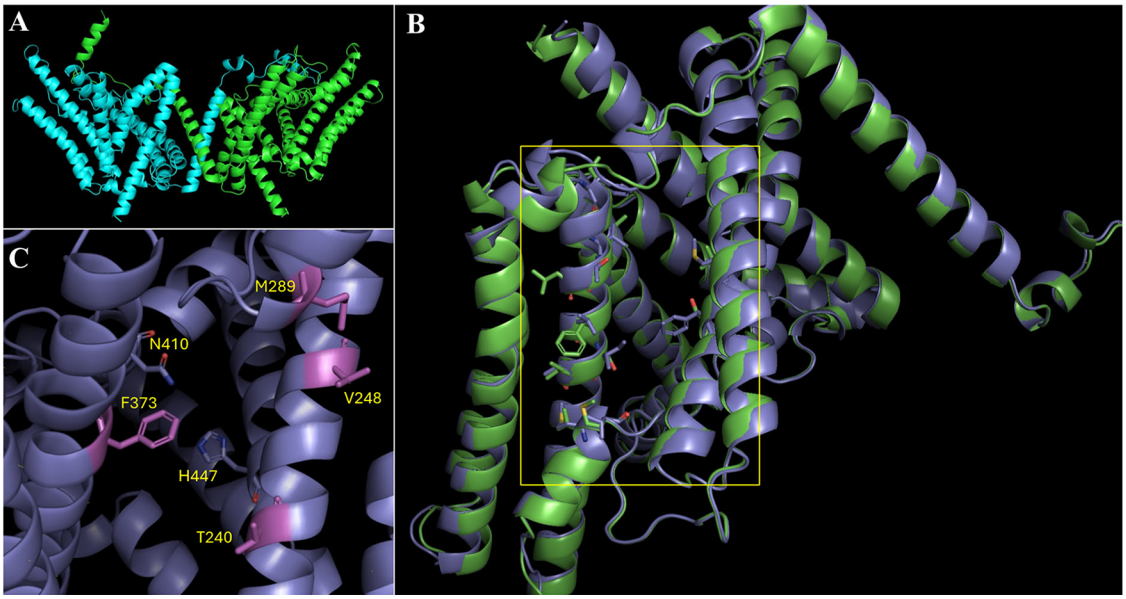

Figure 2. 3D structural model of AtDGAT. (A) Dimeric model showing the overall structure and dimeric interactions between domains. (B) Alignment of AtDGAT (blue) and EgDGAT (green) 3D structural models. The putative fatty acy binding pocket is highlighted with a yellow box. The 10 sites lining the binding pocket identified for characterization is shown in sticks (C) Active site of the enzyme as seen from the lateral gate, featuring the catalytic H447 and N410, as well as the four residue positions (in pink) identified as significant mutation sites (T240, V248, M289, and F373).

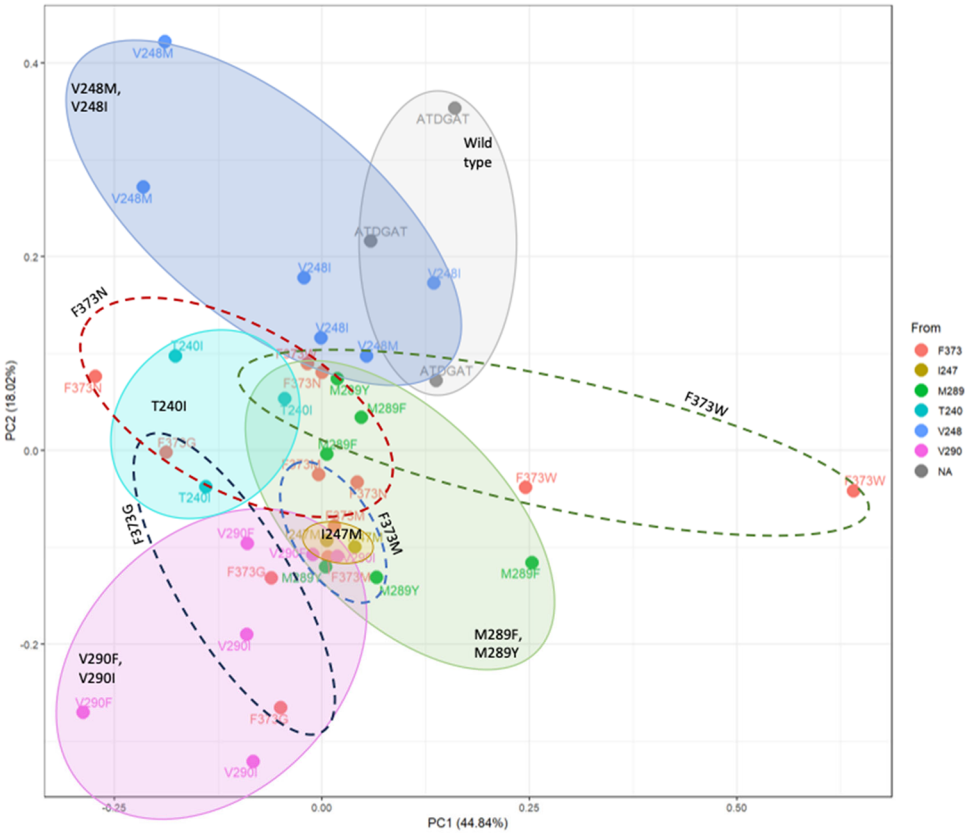

Figure 3. PCA plot of lipid profile for wild type and 12 single mutants of AtDGAT enzyme (3 replicates each). The replicates from the same mutants of F373 site have been circled independently with a dashed line (--). All replicates from different mutants for sites V248 (blue), T240 (cyan), M289 (green), V290 (magenta), and I247 (orange) has been circled in different colors. Wild type replicates have been circled in gray color.

analysis for fatty acid or TG percentages are reported as a percentage of the fatty acids or TG, respectively. V290 mutants showed a large shift in the PCA plot, mostly due to lower amounts of total TAG produced in these mutants. F373G also displayed a clear difference in the PCA plot (Figure 3) mainly owing to a shift in the carbon chain length preference to short-

https://doi.org/10.1021/acssynbio.5c00143
ACS Synth. Biol. XXXX, XXX, XXX−XXX

and medium-chain fatty acids (Figure 4). According to our 3D structural model, amino acid F373 is located at the lateral gate

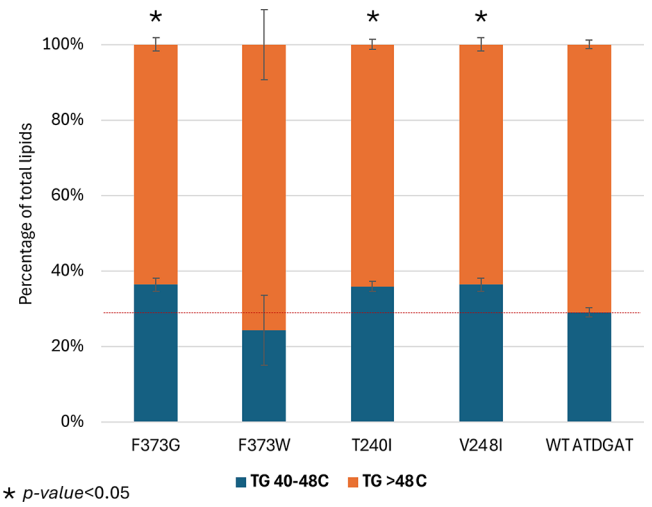

Figure 4. Shift in the carbon chain length profile of fatty acids for four mutants (F373G, F373W, T240I, and V248I) vs wild type AtDGAT. TG 40−48C indicates the percentage of total TAGs with the total carbon number for all three fatty acids in the range of 40−48 (short-/middle-chain fatty acids). TG > 48C indicates the percentage of total TAGs with the total carbon number for all three fatty acids > 48 (longer-chain fatty acids). *p*-value was calculated for all mutants in comparison to the wild type. The standard deviation and *p*-values were calculated from three biological replicates.

of the substrate-binding pocket (Figure 2C) and, hence, is potentially affecting the overall TAG composition. The F373 amino acid is right before the fatty acid binding protein signature motif in the AtDGAT protein sequence[18] and is adjacent to the F374 which has been shown to be part of the substrate-binding pocket in the reported human DGAT1 structure.[55] Multiple sequence alignment shows that at this position 373, amino acid phenylalanine (F) is highly conserved across different plant species but is changed to threonine (T) for *Elaeis guineensis* DGAT, which prefers medium-chain fatty acid.[18] Thus, mutation at this site affects the fatty acid profile of the TAGs produced. The complete breakdown of the TAG profiles has been listed in the Supplemental Figure S5, and enzymatic assays with short-chain acyl-CoA substrates are required for confirming the shift in substrate specificity.

Selective transesterification of *sn-1(3)* by an enzymatic (lipase) reaction and subsequent isolation of the cleaved off *sn-1,3* FAEE fraction further confirm the shift in the fatty acid profile of the TAGs. To the best of our knowledge, no *sn-1(3)* fractionation studies have been performed thus far on DGATs expressed in a yeast (*Saccharomyces cerevisiae*) host. This is mainly because a large amount of biomass is required to generate the amount of lipids needed for the enzymatic action, and subsequent fractionation is challenging, given the low lipid yields in *S. cerevisiae*. Hence, such studies have been limited to the analysis of plant oils and animal fats.[10,11,56] To the best of our knowledge, this is the first reported *sn-1(3)* lipid fractions analyzed from the *Saccharomyces cerevisiae* host. In all samples, four major fatty acids, namely, C16:0, C16:1, C18:0, and C18:1, collectively made up ≥ 97% of total fatty acids detected. *S. cerevisiae* has been reported to have a total fatty acid composition mainly consisting of C16:0, C16:1, C18:0, and C18:1 and with minor amounts of C14:0 and C26:0 under normal growth conditions.[57,58] This is consistent with the fatty acid compositions of the mutants analyzed in this study.

FAME analysis of the *sn-1(3)* fraction revealed that the mutant T240I preferred saturated fatty acids in comparison to the wild type and other mutants tested (Figure 5). There was an increase in the relative percentage of C16:0 and C18:0 fatty acids (respectively, 2.6 and 2.3%) and a statistically significant decrease in the C16:1 fatty acid level (3.5%) for the mutant T240I compared to wild type AtDGAT (Table 1). Palm oil preferentially contains C16:0 at the terminal position (*sn-1,3*) of its TAG,[10] while beef fat[59] and cocoa butter[11] have predominantly C16:0 and C18:0 at the *sn-1,3* positions. Hence, the T240I mutant could potentially be used to create lipids similar to these profiles using yeast hosts, such as *S. cerevisiae*. However, the final fatty acid profile depends on the host in which the DGAT protein is being expressed. Fatty acid profiles would vary significantly depending on the endogenous fatty acid profile in the host.[60] For example, *S. cerevisiae* is rich in C16:0, C16:1, C18:0, and C18:1, whereas plants like *A. thaliana* has a broader range of fatty acids like C18:2 and C18:3.[60] Hence, the expression of these mutants in various hosts could lead to different TAG profiles depending on the available pool of acyl-CoAs. In contrast, yeast cells expressing M289F showed an increase in unsaturated fatty acids (Figure 5), specifically monounsaturated fatty acids (C16:1 and C18:1 increased by 2.7 and 0.7%, respectively compared to wild type), and an accompanying decrease in both C16:0 and C18:0 levels (2.2 and 1.6%, respectively) (Table 2). The growth rate (Figure S6) and the protein expression levels of DGAT (Figure S7) in different mutants were also analyzed. The growth rates were comparable, and also the protein expression of the wild type and mutant DGATs was largely comparable (except for M289Y, which was slightly lower) (Figure S7). The lipid amounts obtained from the mutant M289Y were lower than in other strains with huge variability between replicates. Hence, the data for the M289Y mutant were not included in MS as seen in Table 1, Figures 4, and 5. It should be noted that these shifts in TAG profiles are dependent on the acyl-CoA pool available and are therefore specific to expression of *S. cerevisiae*. Results might not be similar when the DGAT mutants are expressed in other hosts.

TAG Profiling. TAG profiling from MS/MS revealed 18 TAG species defined by their acyl carbon number:double bond (ACN:DB) ranging from TG 42:1 to TG 54:3. They were identified based on ammonium adduct precursor ion $[M+NH_4]^+$ and protonated diacylglycerol $[DG]^+$ ion fragments[47,61] (Supplemental Table S4). Majority of TAGs consisted of 1, 2, or 3 monounsaturated acyls, and few contain polyunsaturated fatty acids with two unsaturated sites. Multiple combinations of different fatty acids that surfaced from the same ACN:DB were unresolved. For example, a single ACN:DB, TG 48:3, precursor ion of 818.7231 *m/z* gave two isobars of TG 16:1/16:1/16:1 and TG 18:1/16:1/14:1. This comes from the observed $[DG]^+$ fragment peak at 547.4633 *m/z* which is match for both [DG 16:1/16:1] and [DG 18:1/14:1]. In some cases, up to six TAG kinds were detected from a single ACN:DB making it a challenging task to analyze and profile all 77 TAGs.

Nonetheless, TAG profiling of mutants with shift in specificity (F373G, M289F, T240I, and V248I) was carried out based on $[DG]^+$ fragment intensity, as has been previously reported.[62] The top 10 TAGs with sum of $[DG]^+$ fragment intensities higher than the wild type by at least 20% (≥1.2

https://doi.org/10.1021/acssynbio.5c00143
ACS Synth. Biol. XXXX, XXX, XXX−XXX

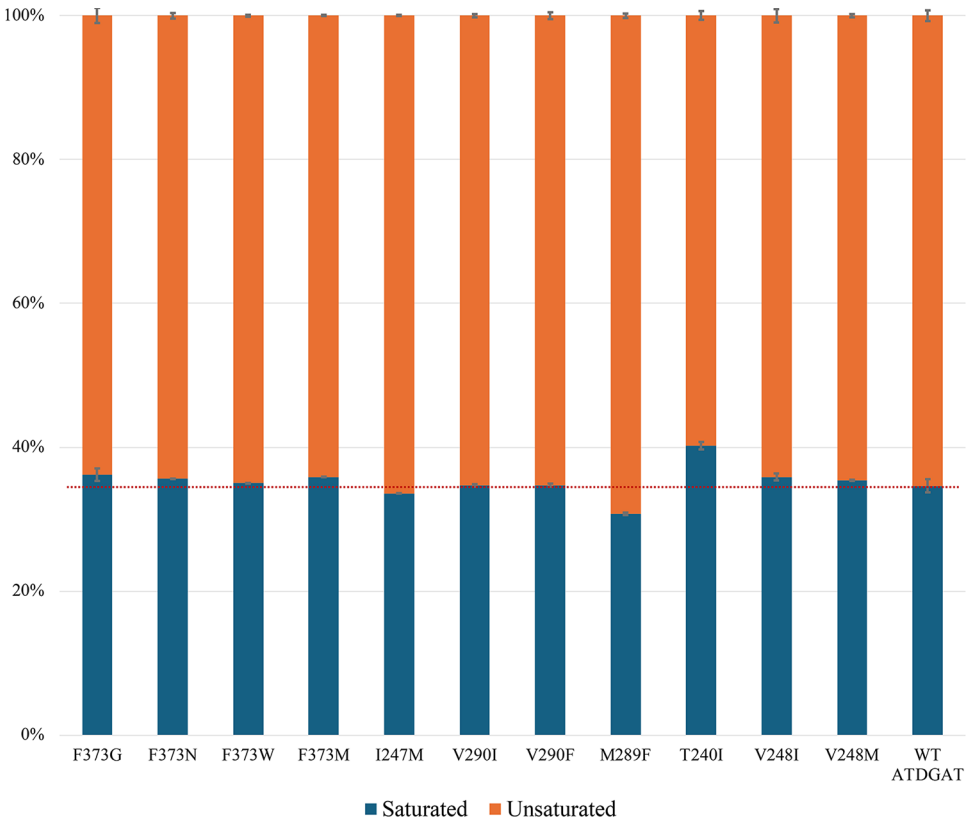

Figure 5. Shift in the substrate preference of the DGAT enzyme in terms of saturation of the carbon chain lengths of the fatty acids at the *sn-1(3)* position of the TAG. "Saturated" indicates the total amount of saturated fatty acids and "Unsaturated" indicates the total amount of unsaturated fatty acids at the *sn-1(3)* position detected through FAME analysis after cleavage of *sn-1,3* fatty acids from TAG backbone. The red dash line (---) indicates the level of saturation of the wild type AtDGAT for comparison purpose. The standard deviations and *p*-values were calculated from two replicates per mutant.

Table 1. Fatty Acid Profile of *sn-1,3* Fraction of Total TAG for DGAT Mutants and Wild Type DGAT[a]

	% content of *sn-1,3* fatty acids (n = 2)					
	C16	C16:1	C18	C18:1	others; saturated	others; unsaturated
wild type	16.86 ± 0.05	28.29 ± 0.52	15.02 ± 0.24	36.14 ± 0.29	2.40 ± 0.08	1.30 ± 0.13
F373G	**17.67 ± 0.02**	27.05 ± 0.13	15.39 ± 0.01	36.09 ± 0.03	2.62 ± 0.12	1.17 ± 0.02
F373N	17.04 ± 0.10	27.53 ± 0.23	15.49 ± 0.05	35.96 ± 0.35	**2.57 ± 0.08**	1.40 ± 0.06
F373W	17.21 ± 0.12	29.43 ± 0.34	14.53 ± 0.06	34.63 ± 0.45	2.83 ± 0.02	1.38 ± 0.06
F373M	**17.50 ± 0.01**	28.46 ± 0.07	15.16 ± 0.04	35.02 ± 0.06	**2.70 ± 0.09**	1.16 ± 0.05
I247M	16.07 ± 0.10	28.71 ± 0.39	14.83 ± 0.01	**36.77 ± 0.30**	2.22 ± 0.04	1.41 ± 0.15
V290I	17.36 ± 0.14	29.02 ± 0.08	14.41 ± 0.07	**35.53 ± 0.29**	**2.51 ± 0.07**	1.16 ± 0.07
V290F	17.45 ± 0.05	29.42 ± 0.32	14.14 ± 0.07	**35.41 ± 0.31**	2.53 ± 0.02	1.05 ± 0.00
M289F	14.67 ± 0.17	31.01 ± 0.84	13.45 ± 0.11	36.77 ± 1.30	2.35 ± 0.03	**1.75 ± 0.14**
T240I	19.42 ± 0.31	**24.79 ± 0.25**	17.42 ± 0.22	34.44 ± 0.94	**2.75 ± 0.06**	1.18 ± 0.21
V248I	17.24 ± 0.13	26.00 ± 0.23	15.81 ± 0.00	**37.36 ± 0.36**	2.47 ± 0.13	**1.12 ± 0.13**
V248M	17.64 ± 0.19	28.70 ± 0.18	14.86 ± 0.36	35.21 ± 0.47	2.54 ± 0.01	1.05 ± 0.02

[a]The percentages with significant difference (p-value < 0.05) compared to the wild type calculated through student t-test has been highlighted in bold.

times) were identified (Table 2). Among these, two different 50:3 TAGs (18:1/18:1/14:1, 16:1/16:1/18:1) were the top differentiators, with the former found to be least in the wild type. Additionally, four new TAGs were detected in the mutant(s) at meaningful intensities (sum $[DG]^+ \geq 1000$), namely, TG 18:0/16:0/14:1 (48:1), TG 16:0/16:0/18:2 (50:2), TG 16:1/16:1/20:0 (52:2), and TG 16:1/16:1/20:1 (52:3), with the first two exclusively surfacing in T240I and M289F, respectively.

M289F preference for MUFA was observed in medium-/longer-chain TAGs, i.e., TG 16:1/16:1/16:1 (48:3), TG 18:1/16:1/14:1 (48:3), and TG 18:1/18:1/14:0 (50:2) (Table 2). Meanwhile, the T240I preference for saturated FAs was observed mainly in TG 48:1, with shorter saturated fatty acids present in TG 16:0/16:0/16:1 and TG 18:1/16:0/14:0 (Table 2). Interestingly, elevated levels of 18:1 in V248I from *sn-1,3* (Table 1) are not reflected in TG 18:1/18:1/18:1 (54:3) but rather in at least four other TGs: TG 18:1/18:1/14:0 (50:2);

https://doi.org/10.1021/acssynbio.5c00143
ACS Synth. Biol. XXXX, XXX, XXX−XXX

Table 2. List of TAG Species Analyzed through MS/MS Based on $[DG]^+$ Fragment Intensity and Their Distribution for Various DGAT Mutants Compared to the Wild Type DGAT[a]

Retention time (min)	TAG*	[DG]+ fragment ions
13.47	TG 48:1 TG 16:0/16:0/16:1	
13.47	TG 48:1 TG 18:1/16:0/14:0	
9.87	TG 48:3 TG 16:1/16:1/16:1	
9.87	TG 48:3 TG 18:1/16:1/14:1	
16.44	TG 50:1 TG 18:0/18:1/14:0	
13.93	TG 50:2 TG 18:1/16:0/16:1	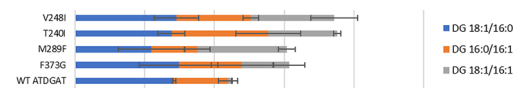
13.93	TG 50:2 TG 18:1/18:1/14:0	
11.87	TG 50:3 TG 16:1/16:1/18:1	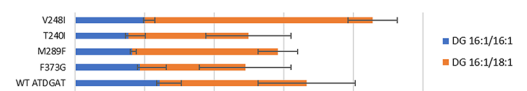
20.87	TG 54:2 TG 18:1/18:1/18:0	

[a]FA positions are interchangeable (non regiospecific).

TG 18:1/18:1/14:1 (50:3); TG 16:1/16:1/18:1 (50:3); and TG 18:1/18:1/18:0 (54:2) (Table 2).

Comparison of Lipid Profiles of H1246 Strains Expressing Various Heterologous DGATs. To gain insights into the substrate preference of DGAT, we expressed various DGAT sequences in the TAG-deficient H1246 yeast strain and tested its effects on the H1246's TAG profile. Specifically, the expression vectors encoding CeDGAT2-2 (*Cyperus esculentus*),[37] TaDGAT2 (*Thraustochytrium aureum*),[38] OsDGAT1-1 (*Oryza sativa*),[39] and AtDGAT1 (*Arabidopsis thaliana*)[26] and the empty expression vector were transformed into H1246 cells. These four DGATs were chosen as they have been reported to have distinct substrate specificities.[37−39] Lipids extracted from the transformants were subjected to total FAME lipid analysis, and the lipid profiles were compared. Strains expressing CeDGAT2-2 showed higher levels of C18:1, while TaDGAT2 reported to have broad specificity did not show any specific preferences (Figure 6), while the AtDGAT1 expressing strain showed higher levels of C16:0 and the OsDGAT1-1 expressing strain showed higher levels of C18:2. Importantly, the overall fatty acid profiles obtained with the expression of different DGATs (Figure 6) aligned well with previous reports in the literature,[26,37−39] thus indicating that the expression in H1246 is a reliable method to determine DGAT's substrate preference. Additionally, the microsome-based DGAT enzyme assays and H1246-based yeast in vivo assays have been shown to be comparable to each other in terms of their indicative substrate specificity, and the results are dependent on the affinity of DGAT toward acyl-CoAs.[63]

The amino acid residues of interest (F373G, M289F, T240I, and V248I) in AtDGAT were also examined in the 3D structural model for AtDGAT (Figure 2C) to understand the basis for the shift in the yeast lipid profile due to mutations. T240 is located along the lateral gate, where the diacylglycerol substrate enters the binding pocket from the membrane. The change from threonine to isoleucine produces both an increase in hydrophobicity and the steric surface, which may act to block longer chains from binding in this region of the DGAT. M289 is located at the very edge of the lateral gate, and it is very difficult to see how the M289F mutation would promote a preference for unsaturation as opposed to saturation (Figure 5). Similarly, V248 is located at the edge of the lateral gate, and V248I has elevated levels of 18:1 (Table 2). It should be noted that both M289 and V248 sites had the lowest number of mutants active (only 6−8) after site saturation mutagenesis.

https://doi.org/10.1021/acssynbio.5c00143
ACS Synth. Biol. XXXX, XXX, XXX−XXX

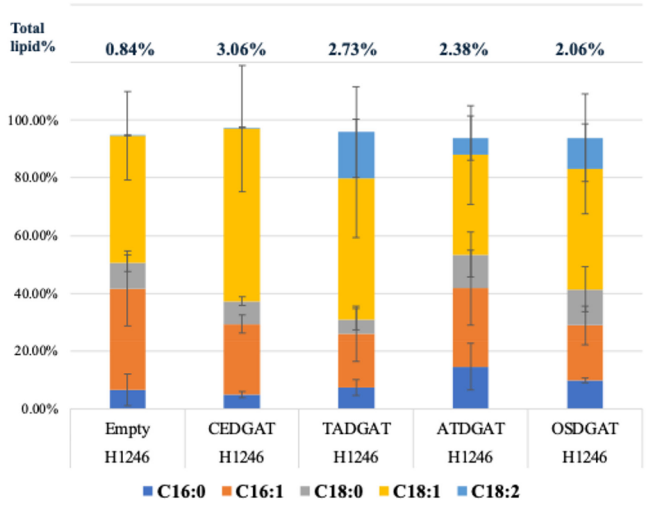

Figure 6. Fatty acid profile for DGAT enzymes with varying reported specificities expressed in the H1246 background strain. Empty indicates empty vector, CEDGAT indicates CeDGAT2-2 from *Cyperus esculentus*, TADGAT indicates TaDGAT2 from *Thraustochytrium aureum*, ATDGAT indicates DGAT1 from *Arabidopsis thaliana*, and OSDGAT indicates OsDGAT1−1 from *Oryza sativa*. (Top) The Total lipid% indicates the amount of lipid as percentage of the total biomass for each strain.

We believe that these positions probably are involved in the dynamics of the enzyme in a way, which cannot be captured in a static model, as described in this study. The F373G mutation removes a bulky hydrophobic group close to the entrance of the lateral gate, which is likely necessary as an interaction site for the flexible longer-chain fatty acids. Thus, its removal might destabilize their interaction with the enzyme, preferring shorter chains instead. Mutating to tryptophan, which is even bulkier than phenylalanine, is therefore more likely to have the reverse effect and prefer longer chains (Figure 4). Some amino acid residues in DGAT have been previously identified that affect the lipid amounts and composition[29] or catalytic activity.[52−54,64] This study focuses on the effect of mutating the residues lining the putative substrate-binding pocket of the DGAT enzyme on the yeast fatty acid profile and subsequently identifies a subset of residues that might be critical for substrate preference. It should be noted that the TAG profile of yeast cells depends not only on the DGAT protein sequence but also on other factors like the protein stability, expression, and cytosolic fatty acid levels.[39,60,65] Even though all of the DGAT mutant proteins were expressed in yeast cells (Figure S7), it is possible that the observed variation in the lipid profile is due to the differences in the levels of the different DGAT proteins. Additionally, if a mutation increases the activity of DGAT, it could alter the TAG composition depending on the available pool of acyl-CoAs in yeast cells. Hence, enzymatic assays would be required to confirm the proposed shift in substrate preference caused by mutations in DGAT.

CONCLUSIONS

The putative substrate-binding pocket of the *Arabidopsis thaliana* DGAT1 enzyme was mutated and characterized to understand the effect of change in the DGAT1 protein sequence on the overall fatty acid profile in yeast. A total of 10 sites were subjected to site saturation mutagenesis, and 192 strains were constructed, of which 127 mutants underwent lipid analysis. This is also the first report of an *sn-1(3)* TAG fraction analysis of lipids from a *Saccharomyces cerevisiae* host overexpressing the DGAT enzyme. Our results show that four different mutations in DGAT, namely, F373G, T240I, M289F, and V248I, shift the overall TAG profile in yeast cells. Hence, these DGAT mutant strains can be potentially utilized to generate customized lipid profiles in yeast. Our results also reconfirm that the DGAT enzyme is crucial for the determination of the overall fatty acid profile in yeasts like *S. cerevisiae*.

ASSOCIATED CONTENT

Data Availability Statement

The data sets generated during and/or analyzed during the current study are available from the corresponding author on reasonable request.

Supporting Information

The Supporting Information is available free of charge at https://pubs.acs.org/doi/10.1021/acssynbio.5c00143..

Codon-optimized AtDGAT (At2g19450) sequence and the primers used; primer list used for site saturation mutagenesis of 10 sites in the AtDGAT sequence; 77 identified TAGs; pESC-GAP-ATDGAT plasmid for the expression of ATDGAT in H1246 cells; overlay of extracted ion chromatograms of triacylglycerols in H1246 strain with empty plasmid vs DGAT; RF cloning random gel electrophoresis check from 190 constructs; TAG profile and PCA analysis for 127 mutants; complete TAG profile of four DGAT mutants F373G, M289F, T240I, and V248I in comparison to the wild type DGAT; growth comparison for 12 mutants, wild type, and the empty vector control; and comparison of the protein expression for 12 mutants, wild type, and the empty vector control (PDF)

AUTHOR INFORMATION

Corresponding Author

Naazneen Sofeo − *Singapore Institute of Food and Biotechnology Innovation (SIFBI), Agency for Science, Technology and Research (A*STAR), Nanos, Singapore 138669*; orcid.org/0000-0001-5724-3394; Email: Naazneen_Sofeo@a-star.edu.sg

Authors

Nazreen V. M. Abdul Muthaliff − *Singapore Institute of Food and Biotechnology Innovation (SIFBI), Agency for Science, Technology and Research (A*STAR), Nanos, Singapore 138669*

Nur Eka Fitriani − *Singapore Institute of Food and Biotechnology Innovation (SIFBI), Agency for Science, Technology and Research (A*STAR), Nanos, Singapore 138669*

Derek Smith − *Singapore Institute of Food and Biotechnology Innovation (SIFBI), Agency for Science, Technology and Research (A*STAR), Nanos, Singapore 138669*

Jing Sen Ong − *Singapore Institute of Food and Biotechnology Innovation (SIFBI), Agency for Science, Technology and Research (A*STAR), Nanos, Singapore 138669*

Lay Kien Yang − *Singapore Institute of Food and Biotechnology Innovation (SIFBI), Agency for Science, Technology and Research (A*STAR), Nanos, Singapore 138669*

https://doi.org/10.1021/acssynbio.5c00143
ACS Synth. Biol. XXXX, XXX, XXX−XXX

Coleen Toledo Busran − *Singapore Institute of Food and Biotechnology Innovation (SIFBI), Agency for Science, Technology and Research (A*STAR), Nanos, Singapore 138669*

Aaron Thong − *Singapore Institute of Food and Biotechnology Innovation (SIFBI), Agency for Science, Technology and Research (A*STAR), Nanos, Singapore 138669;* orcid.org/0000-0003-1852-4067

Prakash Arumugam − *Singapore Institute of Food and Biotechnology Innovation (SIFBI), Agency for Science, Technology and Research (A*STAR), Nanos, Singapore 138669;* orcid.org/0000-0001-6217-8128

Complete contact information is available at: https://pubs.acs.org/10.1021/acssynbio.5c00143

Author Contributions

†N.V.M.A.M. and N.E.F. contributed equally. All authors have given approval to the final version of the manuscript. The credit statement of all authors is as follows: N.V.M.A.M.: methodology, validation, formal analysis, investigation, and writing-original draft. N.E.F.: methodology, software, validation, formal analysis, data curation, investigation, writing-original draft, and visualization. D.S.: conceptualization, methodology, software, validation, investigation, writing-original draft, review, and editing, and funding acquisition. J.S.O. and L.K.Y.: methodology, validation, formal analysis, investigation, and writing-original draft. C.T.B.: methodology, validation, formal analysis, and investigation. A.T.: conceptualization, methodology, writing-review and editing, visualization, supervision, and funding acquisition. P.A.: methodology, writing-review and editing, and supervision. N.S.: conceptualization, methodology, investigation, writing-original draft, review and editing, supervision, project administration and funding acquisition.

Funding

This research is supported by A*STAR project no. C222812021, a Career Development Fund (CDF 2022) from the Agency for Science, Technology, and Research (A*STAR), Republic of Singapore.

Notes

The authors declare no competing financial interest.

■ ACKNOWLEDGMENTS

This research is supported by the A*STAR project no. C222812021, a Career Development Fund (CDF 2022) from the Agency for Science, Technology, and Research (A*STAR), Republic of Singapore. The authors would also like to thank Prof. Sten Stymne (Scandinavian Biotechnology Research, Alnarp, Sweden) for providing the *S. cerevisiae* H1246 strain.

■ REFERENCES

(1) de Carvalho, C. C. C. R.; Caramujo, M. J. The Various Roles of Fatty Acids. *Molecules* **2018**, *23* (10), 2583.

(2) Kao, Y.-C.; Ho, P.-C.; Tu, Y.-K.; Jou, I.-M.; Tsai, K.-J. Lipids and Alzheimer's Disease. *Int. J. Mol. Sci.* **2020**, *21* (4), 1505.

(3) Shahidi, F.; Hossain, A. Role of Lipids in Food Flavor Generation. *Molecules* **2022**, *27*, 5014.

(4) Bajželj, B.; Laguzzi, F.; Röös, E. The Role of Fats in the Transition to Sustainable Diets. *Lancet Planet Health* **2021**, *5* (9), e644−e653.

(5) OECD/FAO. *OECD-FAO Agricultural Outlook 2021−2030*; OECD Publishing, 2021.

(6) Soong, Y.-H. V.; Coleman, S. M.; Liu, N.; Qin, J.; Lawton, C.; Alper, H. S.; Xie, D. Using Oils and Fats to Replace Sugars as Feedstocks for Biomanufacturing: Challenges and Opportunities for the Yeast Yarrowia Lipolytica. *Biotechnol Adv.* **2023**, *65*, No. 108128.

(7) Patel, A.; Karageorgou, D.; Rova, E.; Katapodis, P.; Rova, U.; Christakopoulos, P.; Matsakas, L. An Overview of Potential Oleaginous Microorganisms and Their Role in Biodiesel and Omega-3 Fatty Acid-Based Industries. *Microorganisms* **2020**, *8*, 434.

(8) Salvador López, J. M.; Vandeputte, M.; Van Bogaert, I. N. A. Oleaginous Yeasts: Time to Rethink the Definition? *Yeast* **2022**, *39* (11−12), 553−606.

(9) Mu, H.; Høy, C. E. The Digestion of Dietary Triacylglycerols. *Prog. Lipid Res.* **2004**, 105−133.

(10) Karupaiah, T.; Sundram, K. Effects of Stereospecific Positioning of Fatty Acids in Triacylglycerol Structures in Native and Randomized Fats: A Review of Their Nutritional Implications. *Nutr Metab (Lond)* **2007**, *4*, 16.

(11) Jia, C.-H.; Shin, J.-A.; Lee, K.-T. Evaluation Model for Cocoa Butter Equivalents Based on Fatty Acid Compositions and Triacylglycerol Patterns. *Food Sci. Biotechnol* **2019**, *28* (6), 1649−1658.

(12) Coleman, R. A.; Mashek, D. G. Mammalian Triacylglycerol Metabolism: Synthesis, Lipolysis, and Signaling. *Chem. Rev.* **2011**, *111* (10), 6359−6386.

(13) Yen, C.-L. E.; Stone, S. J.; Koliwad, S.; Harris, C.; Farese, R. V. J. Thematic Review Series: Glycerolipids. DGAT Enzymes and Triacylglycerol Biosynthesis. *J. Lipid Res.* **2008**, *49* (11), 2283−2301.

(14) Banilas, G.; Karampelias, M.; Makariti, I.; Kourti, A.; Hatzopoulos, P. The Olive DGAT2 Gene Is Developmentally Regulated and Shares Overlapping but Distinct Expression Patterns with DGAT1. *J. Exp Bot* **2011**, *62* (2), 521−532.

(15) Shockey, J. M.; Gidda, S. K.; Chapital, D. C.; Kuan, J.-C.; Dhanoa, P. K.; Bland, J. M.; Rothstein, S. J.; Mullen, R. T.; Dyer, J. M. Tung Tree DGAT1 and DGAT2 Have Nonredundant Functions in Triacylglycerol Biosynthesis and Are Localized to Different Subdomains of the Endoplasmic Reticulum. *Plant Cell* **2006**, *18* (9), 2294−2313.

(16) Chawla, K.; Sinha, K.; Neelam; Kaur, R.; Bhunia, R. K. Identification and Functional Characterization of Two Acyl CoA:Diacylglycerol Acyltransferase 1 (DGAT1) Genes from Forage Sorghum (Sorghum Bicolor) Embryo. *Phytochemistry* **2020**, *176*, No. 112405.

(17) Zhou, X.-R.; Shrestha, P.; Yin, F.; Petrie, J. R.; Singh, S. P. AtDGAT2 Is a Functional Acyl-CoA:Diacylglycerol Acyltransferase and Displays Different Acyl-CoA Substrate Preferences than AtDGAT1. *FEBS Lett.* **2013**, *587* (15), 2371−2376.

(18) Aymé, L.; Jolivet, P.; Nicaud, J.-M.; Chardot, T. Molecular Characterization of the Elaeis Guineensis Medium-Chain Fatty Acid Diacylglycerol Acyltransferase DGAT1−1 by Heterologous Expression in Yarrowia Lipolytica. *PLoS One* **2015**, *10* (11), No. e0143113.

(19) Ageitos, J. M.; Vallejo, J. A.; Veiga-Crespo, P.; Villa, T. G. Oily Yeasts as Oleaginous Cell Factories. *Appl. Microbiol. Biotechnol.* **2011**, *90* (4), 1219−1227.

(20) Konzock, O.; Matsushita, Y.; Zaghen, S.; Sako, A.; Norbeck, J. Altering the Fatty Acid Profile of Yarrowia Lipolytica to Mimic Cocoa Butter by Genetic Engineering of Desaturases. *Microb Cell Fact* **2022**, *21* (1), 25.

(21) Shockey, J. M.; Gidda, S. K.; Chapital, D. C.; Kuan, J.-C.; Dhanoa, P. K.; Bland, J. M.; Rothstein, S. J.; Mullen, R. T.; Dyer, J. M. Tung Tree DGAT1 and DGAT2 Have Nonredundant Functions in Triacylglycerol Biosynthesis and Are Localized to Different Subdomains of the Endoplasmic Reticulum. *Plant Cell* **2006**, *18* (9), 2294−2313.

(22) Banilas, G.; Karampelias, M.; Makariti, I.; Kourti, A.; Hatzopoulos, P. The Olive DGAT2 Gene Is Developmentally Regulated and Shares Overlapping but Distinct Expression Patterns with DGAT1. *J. Exp Bot* **2011**, *62* (2), 521−532.

(23) Chawla, K.; Sinha, K.; Neelam; Kaur, R.; Bhunia, R. K. Identification and Functional Characterization of Two Acyl

CoA:Diacylglycerol Acyltransferase 1 (DGAT1) Genes from Forage Sorghum (Sorghum Bicolor) Embryo. *Phytochemistry* **2020**, *176*, No. 112405.
(24) Aymé, L.; Jolivet, P.; Nicaud, J.-M.; Chardot, T. Molecular Characterization of the Elaeis Guineensis Medium-Chain Fatty Acid Diacylglycerol Acyltransferase DGAT1−1 by Heterologous Expression in Yarrowia Lipolytica. *PLoS One* **2015**, *10* (11), No. e0143113.
(25) Xu, R.; Yang, T.; Wang, R.; Liu, A. Characterisation of *DGAT1* and *DGAT2* from *Jatropha Curcas* and Their Functions in Storage Lipid Biosynthesis. *Functional Plant Biology* **2014**, *41* (3), 321−329.
(26) Aymé, L.; Baud, S.; Dubreucq, B.; Joffre, F.; Chardot, T. Function and Localization of the Arabidopsis Thaliana Diacylglycerol Acyltransferase DGAT2 Expressed in Yeast. *PLoS One* **2014**, *9* (3), No. e92237.
(27) Liu, D.; Ji, H.; Yang, Z. Functional Characterization of Three Novel Genes Encoding Diacylglycerol Acyltransferase (DGAT) from Oil-Rich Tubers of Cyperus Esculentus. *Plant Cell Physiol* **2020**, *61* (1), 118−129.
(28) Xu, J.; Francis, T.; Mietkiewska, E.; Giblin, E. M.; Barton, D. L.; Zhang, Y.; Zhang, M.; Taylor, D. C. Cloning and Characterization of an Acyl-CoA-Dependent Diacylglycerol Acyltransferase 1 (DGAT1) Gene from Tropaeolum Majus, and a Study of the Functional Motifs of the DGAT Protein Using Site-Directed Mutagenesis to Modify Enzyme Activity and Oil Content. *Plant Biotechnol J.* **2008**, *6* (8), 799−818.
(29) Zheng, P.; Allen, W. B.; Roesler, K.; Williams, M. E.; Zhang, S.; Li, J.; Glassman, K.; Ranch, J.; Nubel, D.; Solawetz, W.; Bhattramakki, D.; Llaca, V.; Deschamps, S.; Zhong, G.-Y.; Tarczynski, M. C.; Shen, B. A Phenylalanine in DGAT Is a Key Determinant of Oil Content and Composition in Maize. *Nat. Genet.* **2008**, *40* (3), 367−372.
(30) Vanhercke, T.; Dyer, J. M.; Mullen, R. T.; Kilaru, A.; Rahman, Md. M.; Petrie, J. R.; Green, A. G.; Yurchenko, O.; Singh, S. P. Metabolic Engineering for Enhanced Oil in Biomass. *Prog. Lipid Res.* **2019**, *74*, 103−129.
(31) Vanhercke, T.; El Tahchy, A.; Liu, Q.; Zhou, X.-R.; Shrestha, P.; Divi, U. K.; Ral, J.-P.; Mansour, M. P.; Nichols, P. D.; James, C. N.; Horn, P. J.; Chapman, K. D.; Beaudoin, F.; Ruiz-López, N.; Larkin, P. J.; de Feyter, R. C.; Singh, S. P.; Petrie, J. R. Metabolic Engineering of Biomass for High Energy Density: Oilseed-like Triacylglycerol Yields from Plant Leaves. *Plant Biotechnol J.* **2014**, *12* (2), 231−239.
(32) Vanhercke, T.; Divi, U. K.; El Tahchy, A.; Liu, Q.; Mitchell, M.; Taylor, M. C.; Eastmond, P. J.; Bryant, F.; Mechanicos, A.; Blundell, C.; Zhi, Y.; Belide, S.; Shrestha, P.; Zhou, X.-R.; Ral, J.-P.; White, R. G.; Green, A.; Singh, S. P.; Petrie, J. R. Step Changes in Leaf Oil Accumulation via Iterative Metabolic Engineering. *Metab Eng.* **2017**, *39*, 237−246.
(33) Luo, X.-A.; Zhu, Y.-M.; Liu, T.-T.; Wang, X.-P.; Zhou, P.-P.; Bao, Z.-D.; Yu, L.-J. Identification and Characterization of a Novel Diacylglycerol Acyltransferase Gene from Mortierella Alpina. *Biotechnol. Lett.* **2017**, *39* (6), 883−888.
(34) Aymé, L.; Baud, S.; Dubreucq, B.; Joffre, F.; Chardot, T. Function and Localization of the Arabidopsis Thaliana Diacylglycerol Acyltransferase DGAT2 Expressed in Yeast. *PLoS One* **2014**, *9* (3), No. e92237.
(35) Xu, Y.; Chen, G.; Greer, M. S.; Caldo, K. M. P.; Ramakrishnan, G.; Shah, S.; Wu, L.; Lemieux, M. J.; Ozga, J.; Weselake, R. J. Multiple Mechanisms Contribute to Increased Neutral Lipid Accumulation in Yeast Producing Recombinant Variants of Plant Diacylglycerol Acyltransferase 1. *J. Biol. Chem.* **2017**, *292* (43), 17819−17831.
(36) Sandager, L.; Gustavsson, M. H.; Ståhl, U.; Dahlqvist, A.; Wiberg, E.; Banas, A.; Lenman, M.; Ronne, H.; Stymne, S. Storage Lipid Synthesis Is Non-Essential in Yeast *. *J. Biol. Chem.* **2002**, *277* (8), 6478−6482.
(37) Gao, Y.; Sun, Y.; Gao, H.; Chen, Y.; Wang, X.; Xue, J.; Jia, X.; Li, R. Ectopic Overexpression of a Type-II DGAT (CeDGAT2−2) Derived from Oil-Rich Tuber of Cyperus Esculentus Enhances Accumulation of Oil and Oleic Acid in Tobacco Leaves. *Biotechnol. Biofuels* **2021**, *14* (1), 76.
(38) Zhang, C.; Iskandarov, U.; Klotz, E. T.; Stevens, R. L.; Cahoon, R. E.; Nazarenus, T. J.; Pereira, S. L.; Cahoon, E. B. A Thraustochytrid Diacylglycerol Acyltransferase 2 with Broad Substrate Specificity Strongly Increases Oleic Acid Content in Engineered Arabidopsis Thaliana Seeds. *J. Exp Bot* **2013**, *64* (11), 3189−3200.
(39) Bhunia, R. K.; Sinha, K.; Chawla, K.; Randhawa, V.; Sharma, T. R. Functional Characterization of Two Type-1 Diacylglycerol Acyltransferase (DGAT1) Genes from Rice (Oryza Sativa) Embryo Restoring the Triacylglycerol Accumulation in Yeast. *Plant Mol. Biol.* **2021**, *105* (3), 247−262.
(40) Hatanaka, T.; Tomita, Y.; Matsuoka, D.; Sasayama, D.; Fukayama, H.; Azuma, T.; Soltani Gishini, M. F.; Hildebrand, D. Different Acyl-CoA: Diacylglycerol Acyltransferases Vary Widely in Function, and a Targeted Amino Acid Substitution Enhances Oil Accumulation. *J. Exp Bot* **2022**, *73* (9), 3030−3043.
(41) UniProt Consortium. UniProt: The Universal Protein Knowledgebase in 2025. *Nucleic Acids Res.* **2025**, *53* (D1), D609−D617.
(42) Evans, R.; O'Neill, M.; Pritzel, A.; Antropova, N.; Senior, A.; Green, T.; Žídek, A.; Bates, R.; Blackwell, S.; Yim, J.; Ronneberger, O.; Bodenstein, S.; Zielinski, M.; Bridgland, A.; Potapenko, A.; Cowie, A.; Tunyasuvunakool, K.; Jain, R.; Clancy, E.; Kohli, P.; Jumper, J.; Hassabis, D. Protein Complex Prediction with AlphaFold-Multimer. **2022**, bioRxiv 2021.10.04.463034.
(43) Jumper, J.; Evans, R.; Pritzel, A.; Green, T.; Figurnov, M.; Ronneberger, O.; Tunyasuvunakool, K.; Bates, R.; Žídek, A.; Potapenko, A.; Bridgland, A.; Meyer, C.; Kohl, S. A. A.; Ballard, A. J.; Cowie, A.; Romera-Paredes, B.; Nikolov, S.; Jain, R.; Adler, J.; Back, T.; Petersen, S.; Reiman, D.; Clancy, E.; Zielinski, M.; Steinegger, M.; Pacholska, M.; Berghammer, T.; Bodenstein, S.; Silver, D.; Vinyals, O.; Senior, A. W.; Kavukcuoglu, K.; Kohli, P.; Hassabis, D. Highly Accurate Protein Structure Prediction with AlphaFold. *Nature* **2021**, *596* (7873), 583−589.
(44) Mirdita, M.; Schütze, K.; Moriwaki, Y.; Heo, L.; Ovchinnikov, S.; Steinegger, M. ColabFold: Making Protein Folding Accessible to All. *Nat. Methods* **2022**, *19* (6), 679−682.
(45) *PyMOL Molecular Graphics System, Version 3.0*; Schrödinger, LLC, **2025**.
(46) Rostron, K. A.; Lawrence, C. L. *Nile Red Staining of Neutral Lipids in Yeast BT - Histochemistry of Single Molecules: Methods and Protocols*; Pellicciari, C.; Biggiogera, M., Eds.; Springer New York: New York, NY, 2017; pp 219−229.
(47) Watanabe, Y.; Sato, S.; Asada, M.; Arishima, T.; Iida, Y.; Imagi, J.; Saito, K.; Sano, T.; Sasaki, A.; Sasaki, R.; Sato, C.; Shibuya, T.; Tsukahara, Y.; Nagai, T.; Fukazawa, T.; Hori, R.; Homma, R.; Miyazaki, Y.; Yamashita, A.; Yoshinaga, K.; Watanabe, S. Enzymatic Analysis of Positional Fatty Acid Distributions in Triacylglycerols by 1(3)-Selective Transesterification with *Candida Antarctica* Lipase B: A Collaborative Study. *J. Oleo Sci.* **2015**, *64* (11), 1193−1205.
(48) Saini, R. K.; Prasad, P.; Shang, X.; Keum, Y.-S.; Parinandi, L. Molecular Sciences Advances in Lipid Extraction Methods-A Review. *Int. J. Mol. Sci.* **2021**, *22*, 13643.
(49) AOAC. *32.2.02A AOAC Of Fi Cial Method 996.01 Fat (To Tal, Sat u Rated, Un Sat u Rated, and Monounsaturated) in Cereal Products*; AOAC, **2006**; vol *5*.
(50) AOAC. *32.2.02A AOAC Of Fi Cial Method 996.01 Fat (To Tal, Sat u Rated, Un Sat u Rated, and Monounsaturated) in Cereal Products*; AOAC, **2006**; vol *5*.
(51) Sui, X.; Wang, K.; Gluchowski, N. L.; Elliott, S. D.; Liao, M.; Walther, T. C.; Farese, R. V. J. Structure and Catalytic Mechanism of a Human Triacylglycerol-Synthesis Enzyme. *Nature* **2020**, *581* (7808), 323−328.
(52) McFie, P. J.; Stone, S. L.; Banman, S. L.; Stone, S. J. Topological Orientation of Acyl-CoA: Diacylglycerol Acyltransferase-1 (DGAT1) and Identification of a Putative Active Site Histidine and the Role of the n Terminus in Dimer/Tetramer Formation. *J. Biol. Chem.* **2010**, *285* (48), 37377−37387.
(53) Hofmann, K. A Superfamily of Membrane-Bound O-Acyltransferases with Implications for Wnt Signaling. *Trends Biochem. Sci.* **2000**, *25* (3), 111−112.

https://doi.org/10.1021/acssynbio.5c00143
ACS Synth. Biol. XXXX, XXX, XXX−XXX

(54) Chamoun, Z.; Mann, R. K.; Nellen, D.; von Kessler, D. P.; Bellotto, M.; Beachy, P. A.; Basler, K. Skinny Hedgehog, an Acyltransferase Required for Palmitoylation and Activity of the Hedgehog Signal. *Science* **2001**, *293* (5537), 2080−2084.
(55) Wang, L.; Qian, H.; Nian, Y.; Han, Y.; Ren, Z.; Zhang, H.; Hu, L.; Prasad, B. V. V.; Laganowsky, A.; Yan, N.; Zhou, M. Structure and Mechanism of Human Diacylglycerol O-Acyltransferase 1. *Nature* **2020**, *581* (7808), 329−332.
(56) Giuffrida, F.; Marmet, C.; Tavazzi, I.; Fontannaz, P.; Sauser, J.; Lee, L. Y.; Destaillats, F. Quantification of 1,3-Olein-2-Palmitin (OPO) and Palmitic Acid in Sn-2 Position of Triacylglycerols in Human Milk by Liquid Chromatography Coupled with Mass Spectrometry. *Molecules* **2019**, *24* (1), 22.
(57) Viljoen, B. C.; Kock, J. L. F.; Lategan, P. M. Long-Chain Fatty Acid Composition of Selected Genera of Yeasts Belonging to the Endomycetales. *Antonie Van Leeuwenhoek* **1986**, *52* (1), 45−51.
(58) Tuller, G.; Nemec, T.; Hrastnik, C.; Daum, G. Lipid Composition of Subcellular Membranes of an FY1679-Derived Haploid Yeast Wild-Type Strain Grown on Different Carbon Sources. *Yeast* **1999**, *15* (14), 1555−1564.
(59) Rohman, A.; Triyana, K.; Sismindari, S.; Erwanto, Y. Differentiation of Lard and Other Animal Fats Based on Triacylglycerols Composition and Principal Component Analysis. *Int. Food Res. J.* **2012**, *19* (2), 475−479.
(60) Chen, B.; Wang, J.; Zhang, G.; Liu, J.; Manan, S.; Hu, H.; Zhao, J. Two Types of Soybean Diacylglycerol Acyltransferases Are Differentially Involved in Triacylglycerol Biosynthesis and Response to Environmental Stresses and Hormones. *Sci. Rep* **2016**, *6* (1), No. 28541.
(61) Saini, R. K.; Prasad, P.; Shang, X.; Keum, Y.-S. Advances in Lipid Extraction Methods-A Review. *Int. J. Mol. Sci.* **2021**, *22* (24), 13643.
(62) Abed, S. M.; Zou, X.; Ali, A. H.; Jin, Q.; Wang, X. Profiling of Triacylglycerol Composition in Arachidonic Acid Single Cell Oil from Mortierella Alpina by Using Ultra-Performance Liquid Chromatography-Electrospray Ionization-Quadrupole-Time-of-Flight Mass Spectrometry. *Journal of Food Composition and Analysis* **2017**, *62* (July), 245−253.
(63) Roesler, K.; Shen, B.; Bermudez, E.; Li, C.; Hunt, J.; Damude, H. G.; Ripp, K. G.; Everard, J. D.; Booth, J. R.; Castaneda, L.; Feng, L.; Meyer, K. An Improved Variant of Soybean Type 1 Diacylglycerol Acyltransferase Increases the Oil Content and Decreases the Soluble Carbohydrate Content of Soybeans. *Plant Physiol.* **2016**, *171* (2), 878−893.
(64) Lopes, J. L. S.; Nobre, T. M.; Cilli, E. M.; Beltramini, L. M.; Araújo, A. P. U.; Wallace, B. A. Deconstructing the DGAT1 Enzyme: Binding Sites and Substrate Interactions. *Biochim. Biophys. Acta* **2014**, *1838* (12), 3145−3152.
(65) Chen, G.; Xu, Y.; Siloto, R. M. P.; Caldo, K. M. P.; Vanhercke, T.; Tahchy, A. El; Niesner, N.; Chen, Y.; Mietkiewska, E.; Weselake, R. J. High-Performance Variants of Plant Diacylglycerol Acyltransferase 1 Generated by Directed Evolution Provide Insights into Structure Function. *Plant Journal* **2017**, *92* (2), 167−177.

https://doi.org/10.1021/acssynbio.5c00143
ACS Synth. Biol. XXXX, XXX, XXX−XXX